RESEARCH ARTICLE | DECEMBER 03 2024

Textured-piezoelectric-ceramic-based focused intravascular ultrasonic transducer with improved image quality and uniformity

Chaorui Qiu ; Min Su; Shuai Yang ; Baoqiang Liu ; Nanxiang Jia; Zhuo Xu; Hairong Zheng ; Lei Sun ; Weibao Qiu ; Fei Li

Appl. Phys. Lett. 125, 232901 (2024)
https://doi.org/10.1063/5.0237897

Applied Physics Letters ARTICLE pubs.aip.org/aip/apl

Textured-piezoelectric-ceramic-based focused intravascular ultrasonic transducer with improved image quality and uniformity

Cite as: Appl. Phys. Lett. **125**, 232901 (2024); doi: 10.1063/5.0237897
Submitted: 8 September 2024 · Accepted: 20 November 2024 ·
Published Online: 3 December 2024

Chaorui Qiu,[1,2] Min Su,[2,3] Shuai Yang,[1] Baoqiang Liu,[2] Nanxiang Jia,[1] Zhuo Xu,[1] Hairong Zheng,[2] Lei Sun,[3] Weibao Qiu,[2,a)] and Fei Li[1,a)]

AFFILIATIONS

[1]Electronic Materials Research Laboratory, Key Lab of Education Ministry and State Key Laboratory for Mechanical Behavior of Materials, School of Electronic Science and Engineering, Xi'an Jiaotong University, Xi'an 710049, China
[2]Paul C. Lauterbur Research Center for Biomedical Imaging, Shenzhen Institutes of Advanced Technology, Chinese Academy of Sciences, Shenzhen 518055, China
[3]Department of Biomedical Engineering, The Hong Kong Polytechnic University, Hong Kong, China

[a)]**Authors to whom correspondence should be addressed:** wb.qiu@siat.ac.cn and ful5@xjtu.edu.cn

ABSTRACT

Intravascular ultrasound (IVUS) imaging is a minimally invasive medical technology that plays a critical role in diagnosis, treatment guidance, and post-treatment assessment of coronary artery diseases. As a crucial component of the IVUS system, conventional IVUS transducers are designed to be planar and unfocused to adequately cover the region of interest. However, this design comes at the cost of spatial resolution. Here, we developed a high-performance focused IVUS transducer using $Pb(In_{1/2}Nb_{1/2})O_3$-$Pb(Sc_{1/2}Nb_{1/2})O_3$-$PbTiO_3$ (PIN-PSN-PT) textured ceramics with both high electromechanical performance (thickness-mode electromechanical coupling factor k_t: ~60%) and high Curie temperature (T_C: ~250 °C). Benefiting from the relatively low clamped dielectric constant ($\varepsilon_{33}^S/\varepsilon_0$: ~450) of PIN-PSN-PT-textured ceramics in contrast to currently used soft piezoelectric ceramics (>1000), we designed a relatively large aperture for the focused IVUS transducer, with a goal of enhancing lateral resolution across a larger depth of field, ranging from 1 to 5 mm. The developed focused IVUS transducer operates at 42 MHz with an −6 dB bandwidth of 72%, featuring a $0.6 \times 0.6\ mm^2$ aperture while maintaining an electrical impedance of approximately 40–60 Ω. The axial and lateral resolutions characterized by wire phantom imaging are 45 and 208 μm, respectively. The acoustic pressure generated by the focused IVUS transducer is 1.4 times higher than that of its planar counterpart. Ex vivo porcine coronary artery imaging demonstrates that our focused IVUS transducer offers improved image quality and uniformity for the visualization of intravascular structures. Our work shows great potential of PIN-PSN-PT-textured ceramics for creating high-frequency miniaturized focused transducers.

Over the past two decades, cardiovascular diseases have emerged as a prominent global cause of death, severely affecting public health.[1] Atherosclerosis (AS) accounts for a significant portion of cardiovascular diseases, as vulnerable atherosclerotic plaques can rupture at any time, leading to blood clot formation and potentially causing serious complications, such as heart attacks or strokes.[2] Intravascular ultrasound (IVUS) imaging is a minimally invasive diagnostic technique that provides substantial penetration depth and satisfactory resolution, enabling the detection of both the large lipid core (>40% of the plaque's total volume) and thin fibrous cap (<60 μm) of vulnerable plaques.[3–5] This capability makes IVUS imaging crucial for the diagnosis, treatment planning, and post-treatment evaluation of coronary artery diseases.[6,7]

Conventional IVUS imaging relies on a side-looking single-element ultrasonic transducer that is mechanically driven by a rotating motor to provide real-time cross-sectional views of artery walls. Most commercial IVUS transducers operate at frequencies between 20 and 50 MHz, providing an axial resolution of 50–120 μm, a lateral resolution of 300–600 μm, and a penetration depth of 5–15 mm.[8] Further improvements in spatial resolution are necessary to enhance diagnostic accuracy, which places ever-increasing demands on transducer performances. Increasing the operational frequency is a straightforward

approach to improve the spatial resolution. However, ultrasound attenuation in tissues and blood rises significantly with increased frequency, resulting in a notable reduction in penetration depth.[9,10] At a given operational frequency, the axial resolution of IVUS transducers can be improved by increasing their bandwidth,[11] while lateral resolution can be improved by employing acoustic focusing as well as increasing the transducer aperture size.[12–16] However, for practical considerations, the aperture size of IVUS transducer must remain below 0.8 mm to fit into an intravascular catheter.[8] Therefore, the geometries (i.e., aperture size and focal depth) of IVUS transducers require careful design to balance the tradeoffs between lateral resolution and depth of field for optimal imaging performance.

Piezoelectric materials play a pivotal role in transducer performance (i.e., sensitivity and bandwidth). Currently, relaxor-$PbTiO_3$ (PT) single crystals, such as $Pb(Mg_{1/3}Nb_{2/3})O_3$-$PbTiO_3$ (PMN-PT) and $Pb(Zn_{1/3}Nb_{2/3})O_3$-$PbTiO_3$ (PZN-PT), have been extensively utilized in commercial IVUS transducers due to their excellent piezoelectric and electromechanical properties.[12–15,17,18] However, the low phase transition temperature (~100 °C) of relaxor-PT crystals inevitably leads to depolarization during the press-focusing process, because their phase and domain structures become extremely unstable under simultaneous high-temperature and high-pressure conditions, particularly for crystals with compositions near the morphotropic phase boundary.[19,20] Moreover, repolarizing such a thin (<100 μm) crystal plate after the fabrication can degrade transducer performance due to the thickness scaling effect in relaxor-PT crystals.[21,22] Although PZT-5H ceramics exhibit better temperature stability due to their higher Curie temperature (T_C: ~200 °C), their high clamped dielectric constant ($\varepsilon_{33}^S/\varepsilon_0$: >1200) can cause electrical impedance mismatching in focused IVUS transducers with relatively large aperture sizes. For example, the electrical impedance of a PZT-5H ceramic-based focused IVUS transducer with an aperture size of $0.9 \times 0.78\ mm^2$ is approximately 10 Ω, significantly lower than that of the standard electronic system (typically 50 Ω).[23] Such electrical mismatching can lead to inefficient energy transfer and reduced transducer sensitivity, negatively affecting imaging contrast and dynamic range.[24] It is important to note that, for a particular transducer aperture size and frequency, the electrical impedance is determined by the clamped dielectric constant of the piezoelectric material. Therefore, exploring new piezoelectric materials with lower clamped dielectric constants could help mitigate electrical mismatching in focused IVUS transducers that require larger aperture sizes. The fabrication of 1–3 composites is a viable approach to reducing the dielectric constant, yet few studies have reported on high-frequency focused IVUS transducers utilizing 1–3 composites, primarily due to the engineering challenges in geometrically shaping 1–3 composites with thicknesses in the tens of micrometers.[18,25]

Unlike traditional piezoelectric ceramics, where grains are randomly oriented, textured piezoelectric ceramics exhibit a specific grain orientation guided by oriented templates. This structure significantly enhances their piezoelectric and electromechanical properties, making them comparable to piezoelectric single crystals. Additionally, the use of templates (i.e., [001]-oriented $BaTiO_3$) can reduce the dielectric properties of textured ceramics, resulting in higher piezoelectric voltage coefficients (g_{33}).[26] Textured ceramics also offer advantages over single crystals in terms of uniformity, consistency, and cost, making them highly promising for ultrasonic transducers. For instance, Sun *et al.* designed and fabricated a 15-MHz ultrasonic transducers based on $Pb(Mg_{1/3}Nb_{2/3})O_3$-$Pb(Zr, Ti)O_3$ textured ceramics,[27] while Quan *et al.* developed an 80-MHz ultrasonic transducer using lead-free $(K,Na)NbO_3$ (KNN)-based textured ceramics.[28] However, these textured ceramics pose challenges for impedance matching in focused transducers due to their relatively high dielectric constants.

Recently, Yang *et al.* reported novel $Pb(In_{1/2}Nb_{1/2})O_3$-$Pb(Sc_{1/2}Nb_{1/2})O_3$-$PbTiO_3$ (PIN-PSN-PT) textured ceramics, featuring an electromechanical coupling factor of 60%, a moderate clamped dielectric constant of 450, and a high Curie temperature of 250 °C.[29] In this study, we propose using PIN-PSN-PT-textured ceramics to design a focused IVUS transducer, with the aim of improving spatial resolution and enhancing its uniformity over a larger depth of view. The acoustic field distribution was simulated and analyzed to optimize the structural parameters for the focused IVUS transducer. The transducer's performance was evaluated through pulse-echo tests and imaging experiments. Our results indicate that PIN-PSN-PT-textured ceramics hold promise for the development of high-performance focused IVUS transducers with improved imaging capabilities.

The PIN-PSN-PT-textured ceramics were produced via the conventional templated grain-growth method, using the 0.19PIN-0.445PSN-0.365PT powder and 2.5 vol. % [001]-oriented $BaTiO_3$ (BT) templates, as described in Ref. 29. The clamped dielectric constant ($\varepsilon_{33}^S/\varepsilon_0$) was measured at twice of the anti-resonance frequency of the thickness mode. The coercive field (E_C) was determined from the polarization-electric-field (P–E) hysteresis loop measured using a ferroelectric testing system (TF Analyzer 2000E, aixACCT, Germany). The longitudinal wave velocity and thickness-mode electromechanical coupling factor (k_t) were calculated using the resonance method according to the IEEE Standards.[30]

The transducer fabrication followed the methods described by Cannata *et al.*[31] The piezo-ceramic was lapped to a thickness of 38 μm. Cr/Au (thickness: 50/150 nm) electrodes were deposited on both surfaces of the ceramics via DC magnetron sputtering (NSC-3500, NANO-MASTER, USA). The first matching layer and the backing layer had thicknesses of 10 and 400 μm, respectively. After assembling the acoustic stack into a brass housing, a thin layer of parylene (thickness: 12 μm) was vapor-deposited onto the catheter, serving as both the second matching layer and a waterproof coating.

The electrical impedance of the transducer was measured using a precision impedance analyzer (WK6500B, Wayne Kerr Electronics, UK). A conventional pulse-echo test was performed using an ultrasonic pulser/receiver (DR500, JSR Ultrasonics, USA) with a 3-μJ electrical pulse excitation. The acoustic pressure was measured using a hydrophone (NH0500, Precision Acoustics, UK). During the hydrophone test, the transducer was excited by a 5-cycle sinusoidal burst pulse with a peak-to-peak amplitude of 5 V. A 10-μm-diameter tungsten wire phantom and an ex vivo porcine coronary artery were utilized to evaluate the imaging performance. During imaging, the IVUS transducer was rotated by a servomotor through a torque coil with a step size of 0.7°. More details on the imaging system, as well as data acquisition and processing, can be found in our previous work.[32]

Figure 1(a) schematically illustrates the geometry of a spherically focused IVUS transducer. We simulated the acoustic field of the transducers with different geometries using Field II,[33] as shown in Figs. 1(b)–1(e). The geometric focal depth was designed at 2.25 mm. At an aperture size of 0.3 mm, the acoustic field shows no significant change with and without focusing, as the geometric focal depth exceeds the

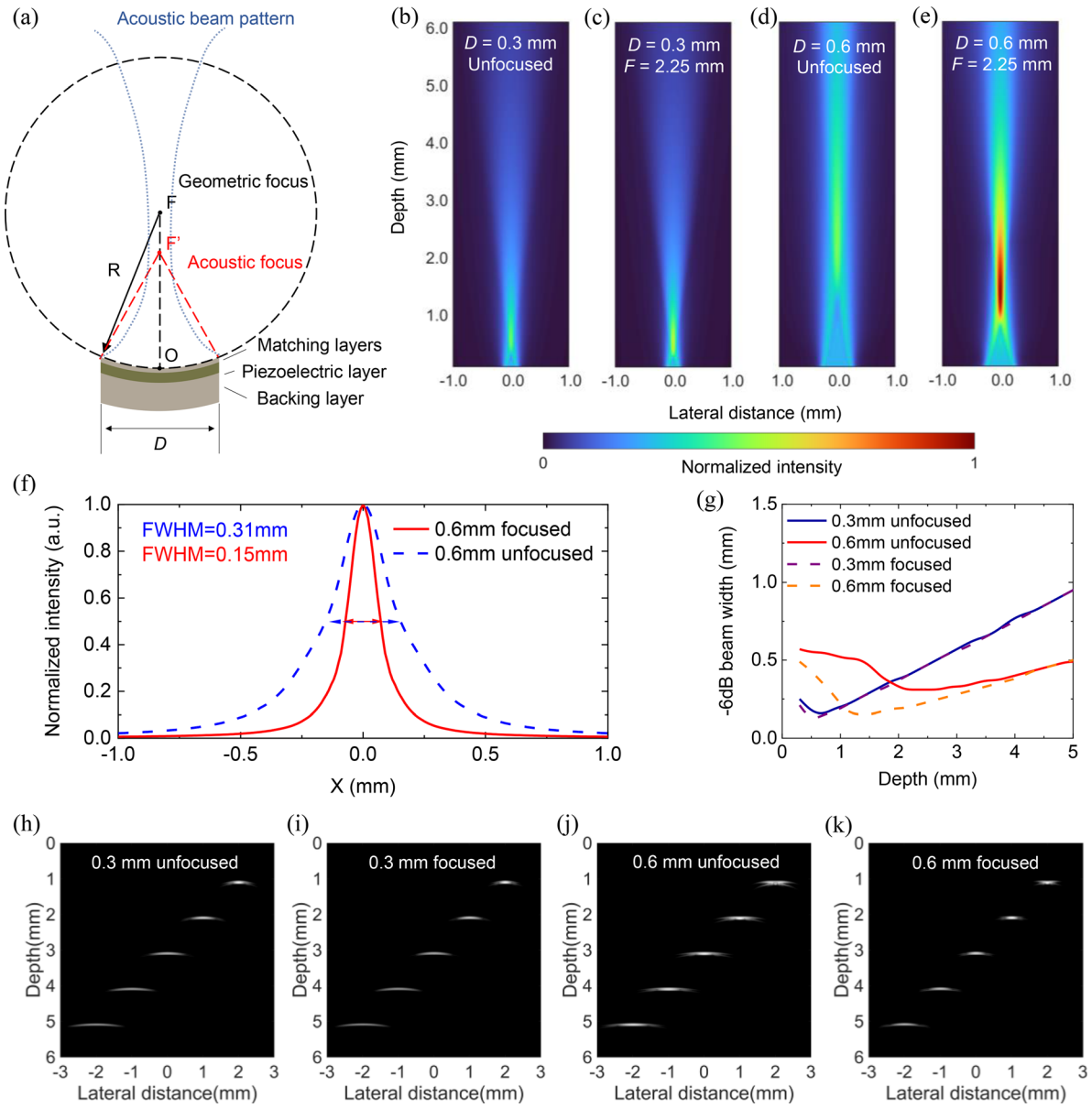

FIG. 1. Simulations for the design of IVUS transducers. (a) Schematic diagram illustrating the geometric structure of the focused IVUS transducer. (b)–(e) Simulated acoustic field distribution for (b) a 0.3-mm focused transducer, (c) a 0.3-mm planar (unfocused) transducer, (d) a 0.6-mm focused transducer, and (e) a 0.6-mm planar transducer. (f) Lateral beam profiles of the 0.6-mm focused and unfocused transducers at their acoustic focal depths. (g) −6 dB beam width as a function of depth. (h)–(k) Simulated ultrasound images of point targets for (h) the 0.3-mm planar transducer, (i) the 0.3-mm focused transducer, (j) the 0.6-mm planar transducer, and (k) the 0.6-mm focused transducer. The point targets are spaced 1 mm apart in the depth direction. The images were normalized to a dynamic range of −40 dB.

natural focal depth (~0.58 mm).[12] When the aperture size is increased to 0.6 mm, the focusing effect becomes prominent, leading to a significant enhancement in acoustic field intensity at a depth of 1.4 mm. Figure 1(f) shows that the 0.6-mm focused transducer exhibits a smaller −6 dB beam width at the acoustic focus compared to the planar counterpart. Figure 1(g) demonstrates the −6 dB beam width with respect to depth for transducers with different geometries. The beam width is minimized at the acoustic focus and then rapidly increases as depth increases. Notably, the 0.6-mm focused transducer has a narrower beam width in the 1–5 mm depth range, which is crucial for IVUS imaging.

We further simulated the imaging performance using a series of point targets, as shown in Figs. 1(h)–1(k). Compared with other transducers, the 0.6-mm focused transducer exhibits superior lateral resolution from 1 to 5 mm. This improvement is attributed to the narrower beam pattern resulting from the focusing effect. It should be noted that

the lateral resolution of the 0.3-mm transducer significantly degrades as imaging depth increases, primarily due to the divergence of the acoustic beam.[34] Therefore, developing a focused IVUS transducer with a relatively larger aperture can not only significantly increase the acoustic field intensity at the focus but also improve the lateral resolution and its uniformity in the region of interest for IVUS imaging.

Figures 2(a) and 2(b) show the microstructure of PIN-PSN-PT-textured ceramics using scanning electron microscope (SEM) and x-ray diffraction (XRD). The SEM image [Fig. 2(a)] displays crystalline grains growing along the [001] direction, guided by [001]-oriented $BaTiO_3$ (BT) templates marked by red arrows. Only the (001) characteristic peaks of the perovskite structure can be observed from the XRD pattern [Fig. 2(b)], indicating a high degree of texturing, which contributes to the excellent electromechanical performance of PIN-PSN-PT-textured ceramics.[29,35] Figures 2(c) and 2(d) present the polarization-electric-field hysteresis (P-E) loop and temperature-dependent dielectric constant of PIN-PSN-PT-textured ceramics, respectively. The coercive field is 6 kV cm^{-1}, and the Curie temperature is 250 °C, indicating the good stability of PIN-PSN-PT-textured ceramics.

We summarized the properties of PIN-PSN-PT-textured ceramics and other contemporary piezoelectric materials in Table I. Currently, piezoelectric materials for IVUS transducers can be classified into three main categories. The first category includes PNN-PZT-based ceramics, Sm-PMN-PT ceramics, and PMN-PZT textured ceramics. These materials exhibit high clamped dielectric constants, typically between 1500 and 3000, making them suitable for 35–45 MHz miniaturized IVUS transducers with apertures smaller than 0.4 mm. The second category includes relaxor-PT crystals and PZT-5H ceramics, which have clamped dielectric constants between 800 and 1200. These materials are ideal for 35–45 MHz IVUS transducers with apertures between 0.4 and 0.5 mm. The third category is LN crystals, characterized by an extremely low dielectric constant, which makes them suitable for ultrahigh-frequency (>80 MHz) miniaturized IVUS transducers. In comparison, PSN-PMN-PT-textured ceramics exhibit a lower clamped dielectric constant than PIN-PMN-PT crystals but significantly higher than LN crystals, making them well-suited for 35–45 MHz IVUS transducers with apertures larger than 0.5 mm or for 45–60 MHz miniaturized transducers. Additionally, while PIN-PSN-PT-textured ceramics have dielectric properties comparable to hard-PZT ceramics, they exhibit a higher electromechanical coupling factor (k_t), which is advantageous for achieving broader bandwidth and higher sensitivity.

Figure 3(a) illustrates a schematic diagram of the focused IVUS catheter, which comprises a focused acoustic stack, brass housing, torque coil, and coaxial cable. Based on our simulations, we selected an aperture size of 0.6 mm for the transducer. To achieve the desired spherical-focused shape, a $0.6 \times 0.6\,mm^2$ planar acoustic stack was placed into a silicone rubber mold and pressed by a stainless-steel cover while being heated to 100 °C, as schematically shown in Fig. 3(b). Figure 3(c) shows a cross section of the IVUS catheter. Figures 3(d) and 3(e) display the focused and planar acoustic stacks assembled in the brass housings, respectively. Figure 3(f) shows a fully assembled IVUS catheter, along with the torque coil and built-in slip ring.

Figures 4(a) and 4(b) show the frequency-dependent electrical impedance of the acoustic stacks before and after press-focusing, respectively. The impedance values for both the planar and focused stacks range from approximately 40 to 60 Ω, which satisfy the requirement for 50-Ω electrical impedance matching. Figures 4(c) and 4(d)

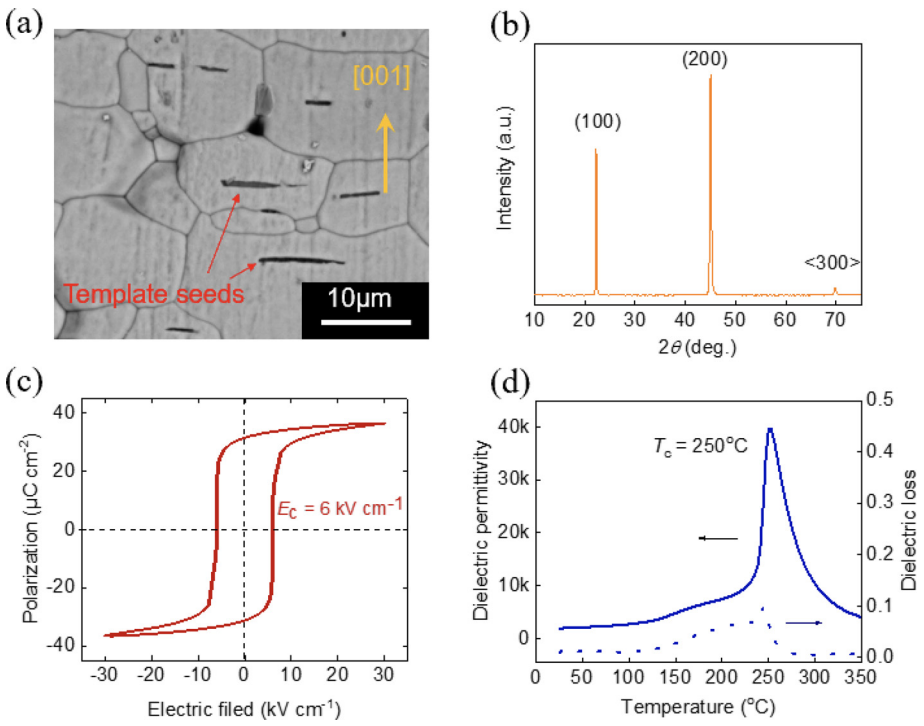

FIG. 2. Microstructure and properties of PIN-PSN-PT-textured ceramics. (a) SEM image of the fracture surface. (b) XRD pattern, (c) P-E loop, and (d) temperature dependent dielectric constant at 1 kHz. The red arrows in (a) indicate the [001]-oriented BT template seeds within the crystalline grains.

TABLE I. Comparisons of piezoelectric materials for IVUS transducers.

Materials	Relative clamped permittivity, $\varepsilon^s/\varepsilon_0$	Electromechanical coupling factor, k_t	Longitudinal velocity, v_l (m s^{-1})	Curie/phase transition temperature (°C)	Coercive field (kV cm^{-1})	Suitable applications
PNN-PZT based ceramics	3400	0.6	3880	113	···	35–45 MHz
Sm-PMN-PT ceramics	3000	0.54	4450	100	3.0	<0.4 mm IVUS transducer
PMN-PZT textured ceramics[28]	2310	0.69	3600	···	···	
KNLN-BZ-BNT textured ceramics[35]	1600	0.40	5610	246	11.0	
PZT-5H ceramics (3203HD)[36]	1200	0.55	4760	225	8	35–45 MHz
PMN-PT crystals[37]	850	0.58	4600	90	2.5	0.4–0.5 mm IVUS transducer
PMN-PT-textured ceramics[38]	810	0.56	···	152	3.9	
PIN-PMN-PT crystals[31]	780	0.58	4450	120	4.5	
$LiNbO_3$ crystals[35]	39	0.49	7340	1200	···	>80 MHz IVUS transducer
Hard-PZT ceramics (K1000)[36]	445	0.52	···	325	···	35–45 MHz
PIN-PSN-PT-textured ceramics (this work)	440	0.60	4480	250	6.0	> 0.5 mm IVUS transducer

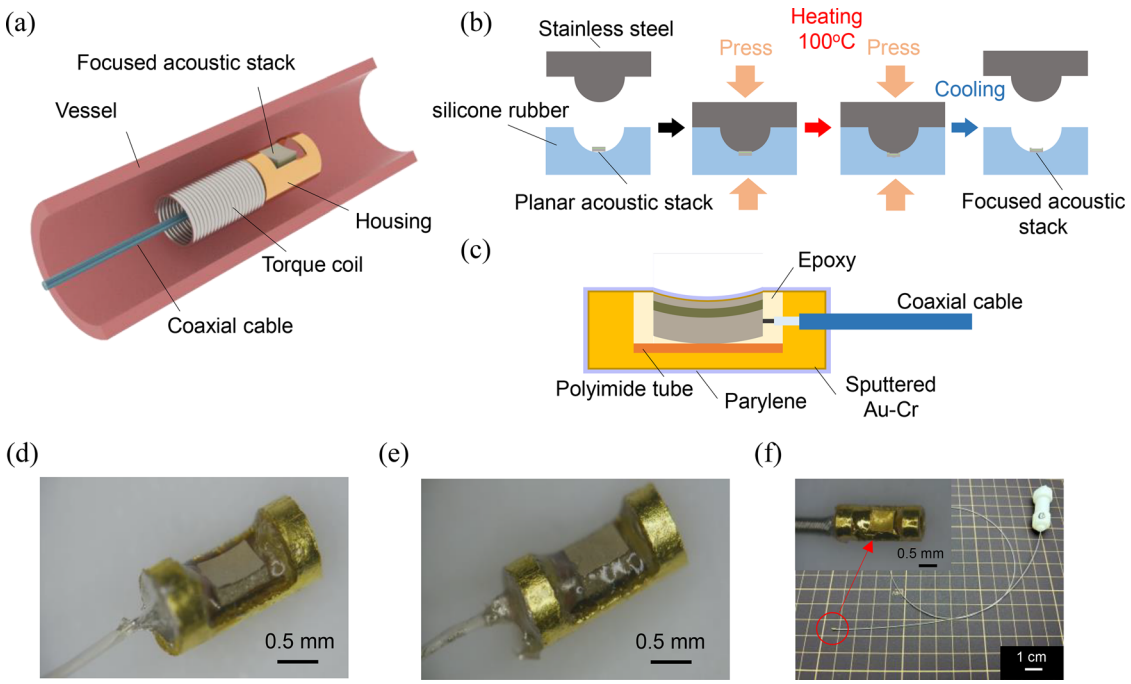

FIG. 3. Schematic diagrams and photos of IVUS transducers. (a) Schematic of the focused IVUS catheter. (b) Fabrication procedure of the focused acoustic stack using a modified press-focusing technique. (c) Cross section of the focused IVUS transducer. (d) and (e) Photos of the as-fabricated focused and planar IVUS transducers, respectively. (f) Photo of the fully assembled focused IVUS catheter.

show the pulse-echo responses and normalized frequency spectra of the planar and focused IVUS transducers, respectively. The peak-to-peak voltages ($V_{p\text{-}p}$) of the unamplified echo signals were 1.8 V for the planar transducer and 1.9 V for the focused transducer. The center frequencies of the planar and focused transducers were calculated to be 41 and 42 MHz, with −6 dB relative bandwidths of 68% and 71%, respectively. The acoustic pressure generated by the focused IVUS transducer was 93.8 kPa, which is 1.4 times higher than that of the planar counterpart, indicating the effectiveness of focusing. Additionally, an abnormal increase in the magnitude and phase of impedance was

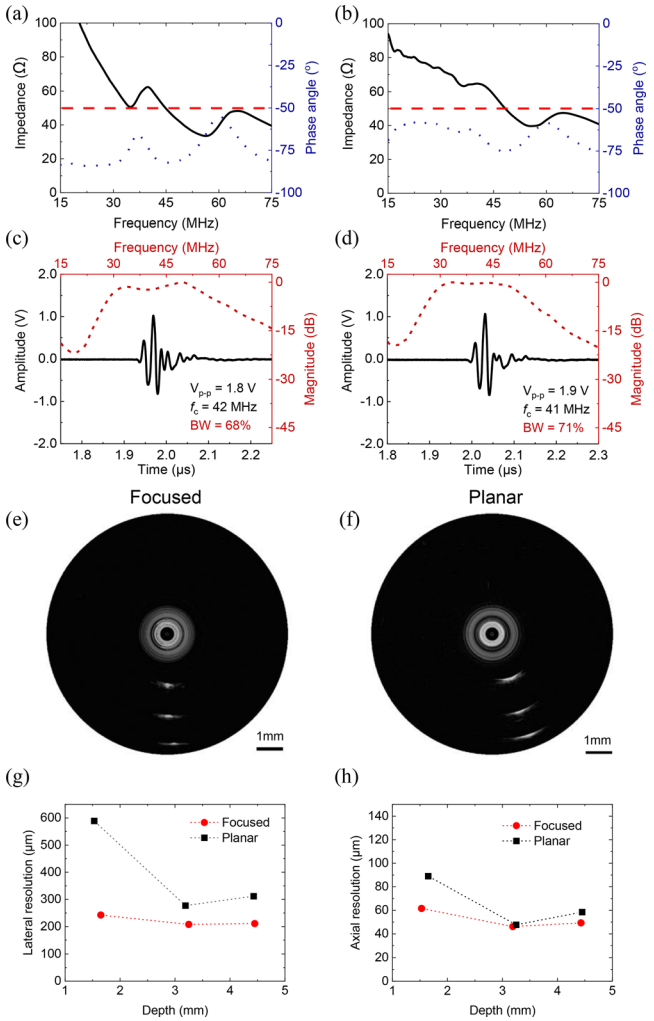

FIG. 4. Characterization of PIN-PSN-PT-textured-ceramic-based transducers. (a) and (b) Frequency-dependent electrical impedance (black solid line) and phase angle (blue dotted line) of the planar and focused acoustic stacks. (c) and (d) Pulse-echo responses (red solid line) and frequency spectra (red dotted line) of the planar and focused IVUS transducers. The red dashed lines indicate an impedance of 50 Ω. (e) and (f) Wire phantom images acquired by the focused and planar IVUS transducers with a dynamic range of 50 dB. (g) and (h) Axial and lateral resolution at different depths for the focused and planar IVUS transducers, respectively.

observed at low frequencies in the focused transducer, which might be attributed to the lateral vibration mode from small cracked fragments generated during press-focusing. However, the transducer's performance is minimally affected by this effect, as evidenced by the pulse-echo results.

Figures 4(e) and 4(f) show the IVUS images of the wire phantom acquired using the planar and focused IVUS transducers, respectively. Figures 4(g) and 4(h) display the axial and lateral resolutions as functions of depth, respectively. The focused transducer consistently provides superior lateral and axial resolutions compared to the planar transducer. Table II compares the simulated and measured spatial resolutions at a depth of 3 mm for both the focused and planar transducers.

TABLE II. Comparison of simulated and measured spatial resolutions at a depth of 3 mm for the planar and focused IVUS transducers.

	Axial resolution (μm)		Lateral resolution (μm)	
	Simulated	Measured	Simulated	Measured
Focused	41	45	203	208
Planar	42	48	243	282

To further evaluate the imaging performance of the developed transducers, we conducted *ex vivo* imaging of a porcine coronary artery. Figures 5(a)–5(c) show cross section images of the coronary artery acquired by the PIN-PSN-PT-textured-ceramic-based focused and planar IVUS transducers, and a traditional PZT-5H-ceramic-based planar IVUS transducer, respectively.[39] The focused transducer provided the clearest distinction of the tunica intima and excellent imaging contrast, due to its superior spatial resolution and sensitivity. The contrast-to-noise ratio (CNR) of the focused and planar transducer was calculated to be 31.7 and 20.2, respectively, indicating the better imaging quality of the focused transducer. It is noteworthy that the PZT-5H-ceramic-based transducer exhibited significantly inferior imaging contrast, limiting the detectable tissue depth to less than 0.6 mm. In contrast, the PIN-PSN-PT-textured ceramic-based focused and planar transducers enable visualization of tissues with thicknesses of approximately 1 and 0.9 mm, respectively, under the same conditions. These results indicate that PIN-PSN-PT-textured ceramic-based focused IVUS transducers can improve image quality and uniformity across a large depth of field.

We compared the performance of our IVUS transducers with those reported in other studies, as shown in Table III. Our PIN-PSN-PT-textured-ceramic-based IVUS transducers demonstrate comparable bandwidth and axial resolution to those reported in similar studies, with improved lateral resolution due to focusing. The PNN-PZT-ceramic-based transducer shows the highest lateral resolution because of its smaller aperture size, which enhances lateral resolution at shallow depths.

In summary, we have developed a high-performance focused IVUS transducer based on PIN-PSN-PT-textured ceramics with superior electromechanical performance. Owing to the moderate clamped dielectric constant of PIN-PSN-PT-textured ceramics, the IVUS transducer possesses an appropriate electrical impedance of around 50 Ω, even with a relatively large aperture size of $0.6 \times 0.6\,\text{mm}^2$. The optimal electrical matching and geometrical focusing significantly improved imaging quality and uniformity during *ex vivo* porcine coronary artery imaging, compared to the traditional PZT-5H-ceramic-based counterpart. The spatial resolution of the PIN-PSN-PT-textured-ceramic-based transducers can be further improved by proportionately increasing the center frequency and decreasing the aperture size while maintaining a satisfactory electrical impedance for optimal transducer sensitivity. Compared to relaxor-PT crystals, the lower clamped dielectric constant and comparable electromechanical property make PIN-PSN-PT-textured ceramics a better choice for IVUS transducers that require a larger aperture size or higher frequency. Furthermore, the

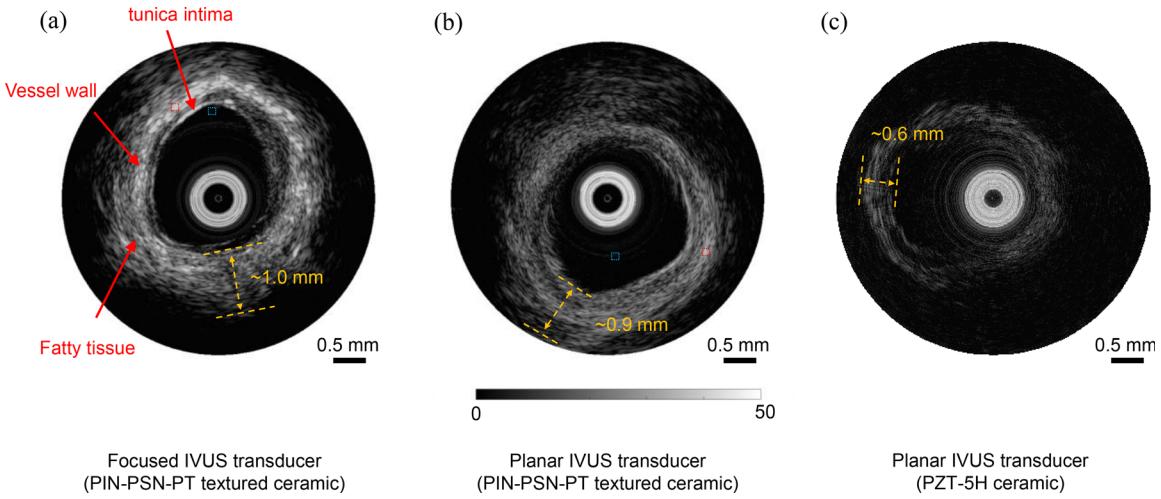

FIG. 5. Ex vivo imaging of a porcine coronary artery using different IVUS transducers. (a) Focused PIN-PSN-PT-textured-ceramic-based transducer. (b) Planar PIN-PSN-PT-textured-ceramic-based transducer. (c) Traditional 40-MHz planar PZT-5H-ceramic-based transducer. The images are displayed with a dynamic range of 50 dB. The red and blue dashed boxes indicate the regions of signal and background used for calculating the contrast-to-noise ratio (CNR).

TABLE III. Performance comparison of our focused IVUS transducer with state-of-the-art IVUS transducers.

References	Material	Geometry	Center frequency (MHz)	−6 dB bandwidth (%)	Aperture (mm^2)	Axial resolution (μm)	Lateral resolution (μm)
This work	PIN-PSN-PT-textured ceramic	Focused	42	72	0.6 × 0.6	45	208
Li *et al.*[39]	PMN-PT crystal 1–3 composite	Planar	41	86	0.5 × 0.4	43	226
Lee *et al.*[40]	PZT-5H	Focused	37	62	0.5 × 0.5	58	211
Ma *et al.*[11]	PMN-PT crystal	Planar	44	61	0.4 × 0.5	42	215
Zhang *et al.*[34]	PNN-PZT-based ceramic	Planar	42	79	0.33 × 0.33	36	141

higher Curie temperature and coercive field of PIN-PSN-PT-textured ceramics provide enhanced stability and reliability, making them suitable for use in medical devices.

This work was supported by the National Natural Science Foundation of China (Grant Nos. 52325205, 52302152, 81927808, 82327805, 82327805, 12004411, 12274430, and 12204504), the China Postdoctoral Science Foundation (Grant No. 2023M732759), the National Key R&D Program of China (No. 2023YFC2416400), Shenzhen Science and Technology Program (Nos. KCXFZ20230731093959009, GJHZ20220913142810021, JCYJ20210324101009023, and JSGGZD20220822095602005), Shenzhen Medical Research Funds (No. B2302053), CAS Research Projects (Nos. KFJ-PTXM-012 and 2011DP173015), the Natural Science Foundation of Guangdong Province (No. 2020B1212060051), and Youth Innovation Promotion Association CAS (No. 2018391).

AUTHOR DECLARATIONS

Conflict of Interest

The authors have no conflicts to disclose.

Author Contributions

Chaorui Qiu and Min Su contributed equally to this paper.

Chaorui Qiu: Conceptualization (equal); Formal analysis (equal); Investigation (equal); Methodology (equal); Writing – original draft (equal); Writing – review & editing (equal). **Min Su:** Methodology (equal); Resources (equal); Validation (equal); Writing – review & editing (equal). **Shuai Yang:** Data curation (equal); Methodology (equal); Resources (equal). **Baoqiang Liu:** Data curation (equal); Formal analysis (equal); Validation (equal). **Nanxiang Jia:** Visualization (equal). **Zhuo Xu:** Funding acquisition (equal); Resources (equal); Supervision (equal). **Hairong Zheng:** Funding acquisition (equal); Resources (equal). **Lei Sun:** Resources (equal); Supervision (equal). **Weibao Qiu:** Conceptualization (equal); Funding acquisition (equal); Resources (equal); Supervision (equal). **Fei Li:** Conceptualization (equal); Funding acquisition (equal); Resources (equal); Supervision (equal); Writing – review & editing (equal).

DATA AVAILABILITY

The data that support the findings of this study are available from the corresponding authors upon reasonable request.

REFERENCES

[1]WHO, see https://www.who.int/news-room/fact-sheets/detail/cardiovascular-diseases-(cvds) for "Cardiovascular diseases (CVDs)" (n.d.).
[2]J. A. Ambrose and A. S. Bhullar, "Inflammation and thrombosis in coronary atherosclerosis: Pathophysiologic mechanisms and clinical correlations," EMJ **4**, 71–78 (2019).
[3]N. W. Shammas, Q. Radaideh, W. J. Shammas, G. E. Daher, R. J. Rachwan, and Y. Radaideh, "The role of precise imaging with intravascular ultrasound in coronary and peripheral interventions," Vasc Health Risk Manage. **15**, 283–290 (2019).
[4]M. Naghavi, P. Libby, E. Falk, S. W. Casscells, S. Litovsky, J. Rumberger, J. J. Badimon, C. Stefanadis, P. Moreno, G. Pasterkamp, Z. Fayad, P. H. Stone, S. Waxman, P. Raggi, M. Madjid, A. Zarrabi, A. Burke, C. Yuan, P. J. Fitzgerald, D. S. Siscovick, C. L. de Korte, M. Aikawa, K. E. Juhani Airaksinen, G. Assmann, C. R. Becker, J. H. Chesebro, A. Farb, Z. S. Galis, C. Jackson, I.-K. Jang, W. Koenig, R. A. Lodder, K. March, J. Demirovic, M. Navab, S. G. Priori, M. D. Rekhter, R. Bahr, S. M. Grundy, R. Mehran, A. Colombo, E. Boerwinkle, C. Ballantyne, W. Insull, Jr., R. S. Schwartz, R. Vogel, P. W. Serruys, G. K. Hansson, D. P. Faxon, S. Kaul, H. Drexler, P. Greenland, J. E. Muller, R. Virmani, P. M. Ridker, D. P. Zipes, P. K. Shah, and J. T. Willerson, "From vulnerable plaque to vulnerable patient: A call for new definitions and risk assessment strategies: Part I," Circulation **108**(14), 1664–1672 (2003).
[5]F. D. Kolodgie, A. P. Burke, A. Farb, H. K. Gold, J. Yuan, J. Narula, A. V. Finn, and R. Virmani, "The thin-cap fibroatheroma: A type of vulnerable plaque: The major precursor lesion to acute coronary syndromes," Curr. Opin. Cardiol. **16**(5), 285–292 (2001).
[6]H. M. García-García, N. Gonzalo, J. F. Granada, E. Regar, and P. W. Serruys, "Diagnosis and treatment of coronary vulnerable plaques," Expert Rev. Cardiovasc. Ther. **6**(2), 209–222 (2008).
[7]J. M. De La and T. Hernandez, "Clinical impact of intravascular ultrasound guidance in drug-eluting stent implantation for unprotected left main coronary disease: Pooled analysis at the patient-level of 4 registries," JACC-Cardiovasc. Interventions **7**(3), 244–254 (2014).
[8]C. Peng, H. Wu, S. Kim, X. Dai, and X. Jiang, "Recent advances in transducers for intravascular ultrasound (IVUS) imaging," Sensors **21**(10), 3540 (2021).
[9]T. Ma, M. Yu, Z. Chen, C. Fei, K. Shung, and Q. Zhou, "Multi-frequency intravascular ultrasound (IVUS) imaging," IEEE Trans. Ultrason., Ferroelectr., Freq. Control **62**(1), 97–107 (2015).
[10]K. K. Shung, *Diagnostic Ultrasound: Imaging and Blood Flow Measurements* (CRC Press, 2015).
[11]X. Ma and W. Cao, "Single-crystal high-frequency intravascular ultrasound transducer with 40-μm axial resolution," IEEE Trans. Ultrason., Ferroelecr., Freq. Control **67**(4), 810–816 (2020).
[12]Q. Zhou, K. H. Lam, H. Zheng, W. Qiu, and K. K. Shung, "Piezoelectric single crystal ultrasonic transducers for biomedical applications," Prog. Mater. Sci. **66**, 87–111 (2014).
[13]C. Fei, Y. Yang, F. Guo, P. Lin, Q. Chen, Q. Zhou, and L. Sun, "PMN-PT single crystal ultrasonic transducer with half-concave geometric design for IVUS imaging," IEEE Trans. Biomed. Eng. **65**(9), 2087–2092 (2018).
[14]Y. Chen, W. B. Qiu, K. H. Lam, B. Q. Liu, X. P. Jiang, H. R. Zheng, H. S. Luo, H. L. W. Chan, and J. Y. Dai, "Focused intravascular ultrasonic probe using dimpled transducer elements," Ultrasonics **56**, 227–231 (2015).
[15]S. Yoon, J. Williams, B. J. Kang, C. Yoon, N. Cabrera-Munoz, J. S. Jeong, S. G. Lee, K. K. Shung, and H. H. Kim, "Angled-focused 45MHz PMN-PT single element transducer for intravascular ultrasound imaging," Sens. Actuators A, Phys. **228**, 16–22 (2015).
[16]J. Lee, J. Jang, and J. H. Chang, "Oblong-shaped focused transducers for intravascular ultrasound imaging," IEEE Trans. Biomed. Eng. **64**(3), 671–680 (2016).
[17]S. Li, J. Tian, and X. Jiang, "A micromachined $Pb(Mg_{1/3}Nb_{2/3})O_3$-$PbTiO_3$ single crystal composite circular array for intravascular ultrasound imaging," ASME J Med. Diagn. **2**(2), 021001 (2019).
[18]X. Li, T. Ma, J. Tian, P. Han, Q. Zhou, and K. K. Shung, "Micromachined PIN-PMN-PT crystal composite transducer for high-frequency intravascular ultrasound (IVUS) imaging," IEEE Trans. Ultrason., Ferroelectr., Freq. Control **61**(7), 1171–1178 (2014).
[19]S. Zhang and F. Li, "High performance ferroelectric relaxor-PbTiO3 single crystals: Status and perspective," J. Appl. Phys. **111**(3), 031301 (2012).
[20]Z. Xu, Z. Xi, F. Chen, Z. Li, L. Cao, Y. Feng, and X. Yao, "Effects of hydrostatic pressure on the dielectric response and phase transition of PMN-PT68/32 single crystal," Ceram. Int. **30**(7), 1699–1701 (2004).
[21]C. Qiu, J. Liu, F. Li, and Z. Xu, "Thickness dependence of dielectric and piezoelectric properties for alternating current electric-field-poled relaxor-PbTiO3 crystals," J. Appl. Phys. **125**(1), 014102 (2019).
[22]H. J. Lee, S. Zhang, J. Luo, F. Li, and T. R. Shrout, "Thickness dependent properties of relaxor-PbTiO(3) ferroelectrics for ultrasonic transducers," Adv. Funct. Mater. **20**(18), 3154–3162 (2010).
[23]M. Su, X. Xia, B. Liu, Z. Zhang, R. Liu, F. Cai, W. Qiu, and L. Sun, "High frequency focal transducer with a Fresnel zone plate for intravascular ultrasound," Appl. Phys. Lett. **119**(14), 143702 (2021).
[24]V. T. Rathod, "A review of electric impedance matching techniques for piezoelectric sensors, actuators and transducers," Electronics **8**(2), 169 (2019).
[25]C. Liu, F. T. Djuth, Q. Zhou, and K. K. Shung, "Micromachining techniques in developing high-frequency piezoelectric composite ultrasonic array transducers," IEEE Trans. Ultrason., Ferroelectr., Freq. Control **60**(12), 2615–2625 (2013).
[26]Y. Yan, Y. U. Wang, and S. Priya, "Electromechanical behavior of [001]-textured Pb(Mg1/3Nb2/3)O3-PbTiO3 ceramics," Appl. Phys. Lett. **100**(19), 192905 (2012).
[27]Y. Sun, L. Jiang, R. Chen, R. Li, H. Kang, Y. Zeng, Y. Yan, S. Priya, and Q. Zhou, "Design and fabrication of 15-MHz ultrasonic transducers based on a textured $Pb(Mg_{1/3}Nb_{2/3})O_3$-Pb(Zr, Ti)O_3 ceramic," IEEE Trans. Ultrason. Ferroelectr. Freq. Control **69**(11), 3095–3101 (2022).
[28]Y. Quan, C. Fei, W. Ren, L. Wang, G. Niu, J. Zhao, J. Zhuang, J. Zhang, K. Zheng, P. Lin, X. Sun, Q. Chen, Z.-G. Ye, and T. Karaki, "Lead-free KNN-based textured ceramics for high-frequency ultrasonic transducer application," IEEE Trans. Ultrason., Ferroelectr., Freq. Control **68**(5), 1979–1987 (2021).
[29]S. Yang, J. Li, Y. Liu, M. Wang, L. Qiao, X. Gao, Y. Chang, H. Du, Z. Xu, S. Zhang, and F. Li, "Textured ferroelectric ceramics with high electromechanical coupling factors over a broad temperature range," Nat. Commun. **12**(1), 1414 (2021).
[30]"IEEE Standard on Piezoelectricity," in *ANSI/IEEE Std 176–1987*, 1–66 (1988).
[31]J. M. Cannata, T. A. Ritter, W.-H. Chen, R. H. Silverman, and K. K. Shung, "Design of efficient, broadband single-element (20–80 MHz) ultrasonic transducers for medical imaging applications," IEEE Trans. Ultrason., Ferroelectr., Freq. Control **50**(11), 1548–1557 (2003).
[32]W. Qiu, X. Wang, Y. Chen, Q. Fu, M. Su, L. Zhang, J. Xia, J. Dai, Y. Zhang, and H. Zheng, "Modulated excitation imaging system for intravascular ultrasound," IEEE Trans. Biomed. Eng. **64**(8), 1935–1942 (2017).
[33]J. A. Jensen and N. B. Svendsen, "Calculation of pressure fields from arbitrarily shaped, apodized, and excited ultrasound transducers," IEEE Trans. Ultrason., Ferroelectr., Freq. Control **39**(2), 262–267 (1992).
[34]Q. Zhang, X. Pang, Z. Zhang, M. Su, J. Hong, H. Zheng, W. Qiu, and K. H. Lam, "Miniature transducer using PNN-PZT-based ceramic for intravascular ultrasound," IEEE Trans. Ultrason., Ferroelectr., Freq. Control **66**(6), 1102–1109 (2019).
[35]S. Yang, L. Qiao, J. Wang, M. Wang, X. Gao, J. Wu, J. Li, Z. Xu, and F. Li, "Full matrix electromechanical properties of textured $Pb(In_{1/2}Nb_{1/2})O_3$-$Pb(Sc_{1/2}Nb_{1/2})O_3$-$PbTiO_3$ ceramic," J. Appl. Phys. **131**(12), 124104 (2022).
[36]CtS, see https://www.ctscorp.com/products/piezoelectric for "State-of-the-art piezoelectric products" (n.d.).
[37]Q. Zhou, X. Xu, J. M. Cannata, H. Ameri, M. S. Humayun, P. Han, and K. K. Shung, "PMN-PT single crystal, high-frequency ultrasonic needle transducers for pulsed-wave Doppler application," IEEE Trans. Ultrason., Ferroelectr., Freq. Control **54**(3), 668–675 (2007).
[38]S. Yang, M. Wang, L. Wang, J. Liu, J. Wu, J. Li, X. Gao, Y. Chang, Z. Xu, and F. Li, "Achieving both high electromechanical properties and temperature stability in textured PMN-PT ceramics," J. Am. Ceram. Soc. **105**(5), 3322–3330 (2022).
[39]B. Liu, M. Su, Z. Zhang, R. Liu, L. Sun, H. Zheng, and W. Qiu, "A novel dual-element catheter for improving non-uniform rotational distortion in intravascular ultrasound," IEEE Trans. Biomed. Eng. **70**(6), 1768–1774 (2023).
[40]J. Lee and J. H. Chang, "A 40-MHz ultrasound transducer with an angled aperture for guiding percutaneous revascularization of chronic total occlusion: A feasibility study," Sensors **18**(11), 4079 (2018).